Applied Surface Science 261 (2012) 473–480

Contents lists available at SciVerse ScienceDirect

Applied Surface Science

journal homepage: www.elsevier.com/locate/apsusc

Influence of the carbon fiber surface microstructure on the surface chemistry generated by a thermo-chemical surface treatment

F. Vautard [a], S. Ozcan [a,*], F. Paulauskas [a], J.E. Spruiell [b], H. Meyer [c], M.J. Lance [d]

[a] Polymer Matrix Composites Group, Materials Science and Technology Division, Oak Ridge National Laboratory, United States
[b] Department of Materials Science and Engineering, University of Tennessee, Knoxville, TN, United States
[c] Microscopy Group, Materials Science and Technology Division, Oak Ridge National Laboratory, United States
[d] Ceramic Science and Technology, Materials Science and Technology Division, Oak Ridge National Laboratory, United States

ARTICLE INFO

Article history:
Received 11 July 2012
Received in revised form 7 August 2012
Accepted 13 August 2012
Available online 28 August 2012

Keywords:
Carbon fiber
Surface chemistry
Surface functionalization
Interface adhesion

ABSTRACT

Carbon fibers made of textile and aerospace grade polyacrylonitrile precursor fibers were surface treated by a continuous gas phase thermochemical treatment. The surface chemistry generated by the surface treatment was characterized by X-ray photoelectron spectroscopy. The surface and the average entire microstructure of the fibers were characterized by Raman spectroscopy and X-ray diffraction, respectively. Depending on the grade of the precursor, the final surface concentration of oxygen was comprised between 14% and 24%, whereas the typical commercial electrochemical surface treatments led to concentrations of around 8% with the same fibers. The final concentration of oxygen was directly correlated to the size of the crystallites which was a function of the grade of the polyacrylonitrile precursor and to the corresponding surface microstructure. The thermochemical surface treatment enabled a better control of the nature of the oxygen-containing functionalities as well. Whatever the grade of the precursor, desired hydroxyl groups and carboxylic acid functionalities were preferably generated, which is observed to be difficult with electrochemical surface treatments.

Published by Elsevier B.V.

1. Introduction

The physico-chemical and mechanical properties of a composite material depend on the properties of the reinforcement material, the matrix and the interface. The properties of the interface are related to the conditions used during the manufacturing (thermal history, pressure, process of impregnation of the fibers by the matrix) [1]. Aside from the type of fiber, factors that influence interfacial adhesion between the matrix and the reinforcement material are mechanical interlocking [2], physical [3–5] and chemical [6] interactions, the presence of defects [7], and remaining stress due to the thermal treatment [8] or the shrinkage of the matrix [9]. It was also demonstrated [10] that surface treatments of carbon fiber act in two ways: some weak boundary layers generated during the carbonization of the precursor are removed and the surface properties are modified in order to monitor one or several of the parameters previously cited. Each type of matrix requires a specific fiber surface treatment in order to achieve adequate interfacial adhesion. Electrochemical surface treatments are still widely used for the industrial production of carbon fibers but a more environmentally friendly, highly effective and energy efficient surface treatment technology is needed. Particularly, a process that does not generate liquid waste is more and more demanded. An oxidation in a gas phase involving mainly ozone appeared to be a surface treatment technology that had the potential to be scaled up for industrial production. Our group recently reported a detailed characterization of the surface properties of carbon fibers that were surface treated with this technology and compared those surface properties with the ones created by a commercial electrochemical surface treatment [11]. The thermochemical surface treatment generated a higher surface density of oxygen-containing functional groups, homogeneously and consistently. The concentration of oxygen was up to 20% according to an X-ray photoelectron spectroscopy (XPS) analysis, in comparison to the 7–8% generated by the electrochemical surface treatment [11]. Unlike the electrochemical surface treatment, the thermochemical surface treatment was able to preferentially create desired hydroxyl groups and carboxylic acid functionalities. A topography adapted to the transfer of load from the matrix to the fiber by mechanical interlocking was created as well, and it did not lower the tensile properties of the single fibers. Some healing effect based on an assumption of removing surface imperfections was even suggested by an analysis of the values of the tensile strength of single fibers at different gauge lengths. Nevertheless, the surface was studied with only one example of high strength carbon fiber. It is necessary to study the surface chemistry that is generated with different types of carbon

* Corresponding author. Tel.: +1 865 241 2158.
E-mail address: ozcans@ornl.gov (S. Ozcan).

0169-4332/$ – see front matter. Published by Elsevier B.V.
http://dx.doi.org/10.1016/j.apsusc.2012.08.038

Table 1
Physical and mechanical properties of the carbon fibers used in this study.

Reference	Diameter (μm)	Density (cc/g)	Tensile strength (GPa)	Tensile modulus (GPa)	Elongation at break (%)
Hextow® IM10 surface treated	4.4	1.79	7.0	303	2.1
Hextow® IM7 surface treated	5.2	1.78	5.7	276	1.8
Hextow® AS4 surface treated	7.1	1.79	4.4	231	1.8
Panex® 35 surface treated	7.2	1.81	4.1	242	1.5
Textile grade PAN surface treated	7.4	1.82	3.3	207	1.5

fibers having different carbon structures and eventually highlight a relationship between the surface chemistry and the original surface carbon structure.

In this study, different types of carbon fibers were surface treated with the same conditions and the surface chemistry generated by the thermochemical surface treatment was characterized. A relationship between the graphitic structure of the surface of the carbon fiber and the final surface density of functional groups was established.

2. Materials and methods

2.1. Surface treatment of the carbon fibers

Industrial grade polyacrylonitrile (PAN) based standard modulus carbon fibers Panex® 35 (50k) produced by Zoltek Co., and aerospace grade PAN based high strength carbon fibers Hextow® AS4 (12k), Hextow® IM7 (12k) and Hextow® IM10 (12k) produced by Hexcel Co. were used in this study. Panex® 35 fibers were neither surface treated nor sized. Another set of textile grade PAN carbon fibers (TexPAN) were manufactured in our laboratory. The fiber properties were not optimized in order to be compared to a commercial product at this stage. The fibers from Hexcel Co. were surface treated and not sized. The surface treatment was continuously removed by a thermal treatment at 1000 °C in a three zone furnace equipped with a quartz tube flushed with high purity nitrogen (99.9%). The heat treatment was followed by a progressive cooling to room temperature still under nitrogen (concentration of oxygen maintained under 500 ppm). The final concentration of oxygen, after the thermal treatment, measured by XPS was 2%. The physical properties of the different references are presented in Table 1.

All fibers were continuously surface treated in a reactive gas phase mix containing mainly ozone. Ozone was produced by a PWB-150 g ozone generator from Plasma Techniques Inc. The residence time of the fibers in the reactive gas phase was 2 min. More information about the surface properties generated by this surface treatment (topography at a micro and nano-scale, surface energy) with Panex® 35 fibers and its influence on the tensile strength of the fibers has already been described [11].

2.2. X-ray diffraction analysis

Wide angle X-ray diffraction was used to characterize the average microstructural parameters of the graphitic structure of the carbon fibers. They were determined from the peak positions of the (0 0 2) reflection near 26° (2θ) and the (1 0 0) reflection near 43° (2θ). These included (a) the spacing between graphene layer planes (d_{002}), (b) the so-called "stack height" of the graphene planes (L_c), (c) the crystal size in the direction parallel to the graphene planes (L_a), and (d) the orientation of the graphene planes relative to the fiber axis. All measurements were made using a fully automated Panalytical Materials Research Diffractometer using Cu Kα radiation (λ = 1.5418 Å) in transmission geometry. The sample consisted of a parallel array of fibers. The breadth of the (0 0 2) reflection was measured on the equator (perpendicular to the fibers), while the breadth of the (1 0 0) reflection was measured in the meridian direction (parallel to the fibers).

L_c was calculated from the line breadth of the (0 0 2) reflection in the 2θ direction using the Debye–Scherrer equation:

$$L_c = \frac{K\lambda}{\beta \cos\theta} \quad (1)$$

where λ is the wavelength of the X-ray source, θ is the Bragg angle, β is the full width at half maximum intensity (FWHM) of the (0 0 2) reflection corrected for instrumental broadening, and K is a constant taken to be 0.9 for the calculation of L_c [12]. The instrumental broadening correction was carried out using the Warren [13] correction according to the following equation:

$$\beta^2 = B^2 = b^2, \quad (2)$$

where B is the measured FWHM of the (0 0 2) reflection and b is the FWHM of a sample with a particle size greater than 2000 Å (200 nm) and exhibiting no measurable particle size broadening. In the present case, a silicon powder was used. An indication of the spatial extent of the coherently diffracting domains in the direction parallel to the graphene planes is measured by the average crystallite size in the direction normal to the (1 0 0) planes. This quantity is referred to as L_a(1 0 0). It was obtained from the line breadth of the (1 0 0) reflection in a manner similar to that just described for the calculation of L_c, except that the constant K in equation (1) was taken equal to 1.8, based on the assumption that the structure is essentially a random layer lattice formed by the turbostratic stacking of graphene planes [14].

2.3. Raman spectroscopy

Raman spectra were collected with a Dilor XY800 microprobe (JY Inc., Edison, New Jersey, USA) with an Innova 308c Ar^+ laser (Coherent Inc., Santa Clara, California, USA) operating at 514.5 nm. Spectra were collected from a ~1 μm diameter spot on 10 different fibers from each sample between 90 cm^{-1} and 4000 cm^{-1}, with a resolution of 2 cm^{-1}. Some concerns about the fitting procedures for the Raman spectra of carbon materials exist. In this study, the spectra were fitted with a combination of Gaussian–Lorentzian curves. Regarding the region of the spectra comprised between 800 cm^{-1} and 2000 cm^{-1}, three peak components were used, located at 1100 cm^{-1}, 1370 cm^{-1} and 1600 cm^{-1} respectively. The intensity, width, position and the fraction of Lorentzian (part in the combination Gaussian–Lorentzian) were allowed to vary. A straight line was used as the baseline.

2.4. X-ray photoelectron spectroscopy

X-ray photoelectron spectroscopy analysis of the carbon fiber surface was carried out with a Thermo Scientific K-Alpha X-ray photoelectron spectrometer equipped with a conventional electron energy analyzer. The latter was operated in the fixed transmission mode at constant pass energy of 200 eV for the survey spectra and 50 eV for the core level spectra. A monochromatic Al K_α source (1486.6 eV) operated at 420 W (14 kV; 30 mA) was used as incident radiation. Photo-emitted electrons were collected at

Table 2
Binding energies of C(1s), O(1s) and N(1s) component peaks used for the fitting of XPS core level spectra.

C(1s)		O(1s)		N(1s)	
Binding energy (eV)	Component peak	Binding energy (eV)	Component peak	Binding energy (eV)	Component peak
284.4 ≪ 284.6	Csp^2	531.2 ≪ 531.4	Ph═O (quinone), Ph—C═O, amides	398.4 ≪ 399.0	Pyridine
284.9 ≪ 285.1	Csp^3	532.0 ≪ 532.2	C═O (ester, anhydride, amide), carboxylic acids	399.4 ≪ 399.8	Amines, amides, nitriles
284.8 ≪ 285.0	C—COOR	532.7 ≪ 532.9	R—OH, C—O—C	400.1 ≪ 400.7	Pyrrolidine, pyridone
285.4 ≪ 285.6	C—N	533.5 ≪ 533.7	Ph—OH, C—O (ester, anhydride)	401.1 ≪ 401.7	Pyridinium, protonated N
286.1 ≪ 286.4	C—O—R, C≡N	534.8 ≪ 535.2	Chemisorbed H_2O	403.7 ≪ 404.3	Shake up
287.4 ≪ 287.6	C═O	536.2 ≪ 536.6	Physisorbed H_2O	405.5 ≪ 405.7	NO_x
288.3 ≪ 288.9	COOR	538.2 ≪ 538.6	Shake up		
290.1 ≪ 290.5	Physisorbed H_20				
291.3 ≪ 291.7	Shake up				

a take-off angle of 90° from the sample and the pressure was about 10^{-7} Pa. The spectrometer energy scale was calibrated with respect to Ag 3d5/2, Au 4f7/2 and Cu 2p3/2 core level peaks, set with binding energies of 368.3, 84.0 and 932.7 eV respectively. All binding energies are referenced to the adventitious C(1s) peak located at 284.6 eV. Instrumental sensitivity factors were taken as C(1s):O(1s):N(1s) equals 0.919:2.449:1.882, respectively. For elemental quantification, the accuracy of the analysis was considered to be ±1%. C(1s), O(1s) and N(1s) core level spectra were fitted to GL functions (product of a Lorentzian by a Gaussian) using Avantage 4.44 software. The background was a Tougaard type for the C(1s) peak and linear for the O(1s) and N(1s) peaks. The parameters controlling the shape of the asymmetric component (graphitic component) were determined with the C(1s) core level spectra of the non-surface treated fiber because of its very low concentration of oxygen. The component peaks position used in C(1s), O(1s) and N(1s) curve fitting are presented in Table 2. Regarding the fitting of the C(1s) peak, there is evidence that two peak components are necessary in order to differentiate sp^2 and sp^3 hybridizations of carbon atoms in carbon materials, either in diamond-like structures [15] or amorphous carbon [16]. Not using a component peak for the sp^3 carbon atoms will lead to an overestimate of the quantity of C-O-R type functional groups. The O(1s) peak was fitted according to peak components suggested by Zielke et al. [17] and Biniak et al. [18]. A significant difference with the component suggested by Zielke et al. [17] is that we did not consider the component peak located at 534.2 eV to be related to carboxylic acids. The N(1s) peak was fitted according to peak components suggested by Alexander and Jones [19] and Biniak et al. [18]. The full width at half maximum (FWHM) of all the component peaks was fixed to 2 eV, except for the Csp^2 and "shake up" component peaks, which were adjusted in order to obtain a fitting as close to the experimental spectrum as possible. The C(1s) peak fitting was done so that the total area of all the oxy-carbonated components could not be higher than the total area of the O(1s) peak and that the total area of all the nitro-carbonated components could not be higher than the total area of the N(1s) peak.

3. Results and discussion

3.1. X-ray diffraction analysis

The characteristics of the average microstructural parameters of the carbon fibers are presented in Table 3. The measured average d-spacing between graphene planes varied between 3.46 Å and 3.51 Å, which corresponds to the characteristic distance existing in turbostratic carbon fiber structures. Even if the alignment of the crystals strongly depends on the process parameters used during the stabilization and carbonization of the fiber, it is clear that a better grade of the precursor fiber and optimized process conditions led to larger crystals (values of L_a below 5 nm for the lower grade PAN fibers and higher than 5 nm for the aerospace grade PAN fibers) and a better alignment of the crystals in the final carbon fiber (misalignment above 18.1° for textile grade PAN fibers and below 17.3° for aerospace grade PAN fibers). Those differences in the size and the alignment of the crystals have a direct influence on the mechanical properties of the corresponding fibers. The tensile strength of carbon fibers is also strongly dependent on the diameter of the fiber, as a smaller diameter leads to a lower probability for the fiber to contain a defect (internal void) that will significantly affect the mechanical properties. As seen in Table 1, the fiber having lower values of the diameter (IM10, IM7) also have higher values of the tensile strength. The tensile elastic modulus of carbon fibers depends on the alignment of the crystals with respect to the fiber axis and on the level of crystallinity of the carbon structure (graphitic, turbostratic, glassy, amorphous, . . .). The fiber with the highest value of the tensile modulus (IM10) has the lowest misalignment of the crystal and the highest value of L_a.

X-ray diffraction gives an average value of the microstructural parameters by analyzing the entire fiber. It is known that carbon fibers can have an internal structure significantly different from the carbon structure located in the external part (core-shell structure), due to several reasons such as the kinetics of diffusion of oxygen during the stabilization of the PAN precursor fibers [20], the difference in draw ratio of fiber during spinning and washing,

Table 3
Average micro-structural parameters of the graphitic structure of the carbon fibers.

Reference	d_{002} (Å)	L_c (nm)	L_a (nm)	Misorientation angle (°)
Hextow® IM10 surface treated	3.49	2.00	6.40	15.3
Hextow® IM7 surface treated	3.51	1.81	5.09	15.3
Hextow® AS4 surface treated	3.50	1.65	5.22	17.3
Panex® 35 surface treated	3.46	1.79	4.93	18.1
Textile grade PAN surface treated	3.50	1.66	4.67	19.7

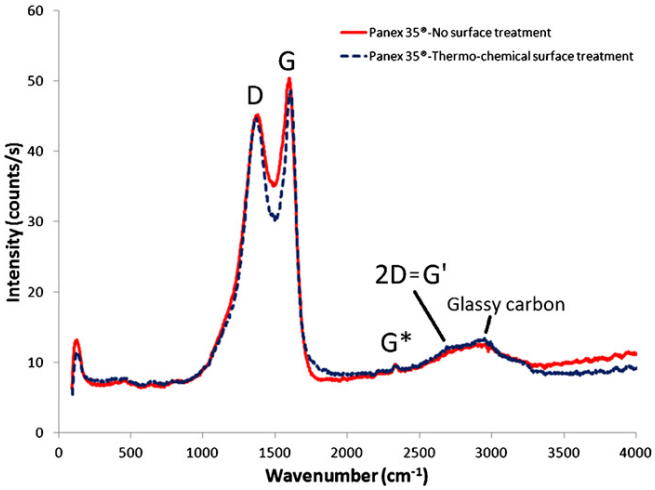

Fig. 1. Raman spectra of Panex® 35 fibers before and after thermochemical surface treatment.

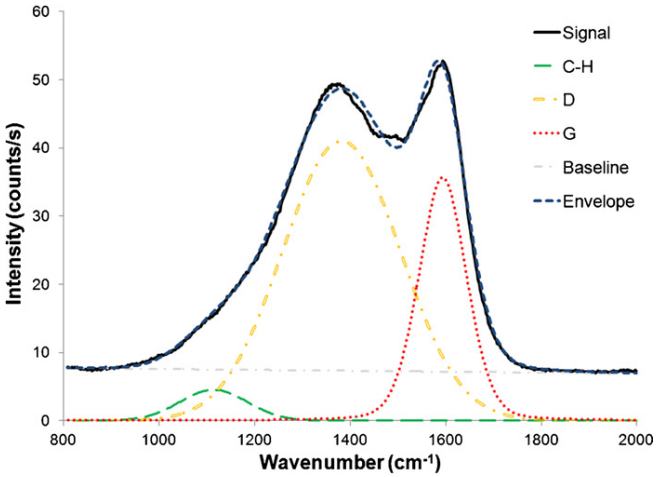

Fig. 2. Fitting of the Raman spectra. Textile grade PAN fibers before surface treatment.

and fiber handling. It was necessary to study the order of graphitization only in the outer layers of the fiber in order to check if there is an influence of the graphitic structure on the generated surface chemistry. Raman spectroscopy relies on the inelastic scattering of a monochromatic light and the depth of analysis in the case of carbon fibers is expected to be below 50 nm. Therefore, Raman spectroscopy is the appropriate analytical technique for surface microstructure characterization. The results related to X-ray diffraction are presented for comparison in the next section.

3.2. Raman spectroscopy

Raman spectroscopy is a widely used technique for the assessment of the disorder existing in the near region surface microstructure of carbon materials, regardless of their origin and their level of graphitization [21]. Bessac et al. [22] listed all the precautions that have to be taken in order to use that technology for a quantitative analysis of the disorder existing in the structure of the surface of carbon fibers, especially the necessity of using a low power for the laser (less than 5 mW), because carbon fibers can be very sensitive to the heat generated by the laser. Subsequently, the location of the peaks can be affected [23]. The Raman spectra of the Panex®35 fibers before and after surface treatment (Fig. 1) are representative of the general aspect of all the spectra that were obtained with the different fibers before and after surface treatment. Since carbon fibers have a graphite-like structure containing a significant amount of turbostratic disorder, it is expected to find two large peaks: a peak located at 1580–1600 cm^{-1} (G peak) due to graphitic in-plane vibrations with E_{2g} symmetry involving an in-plane bond-stretching motion of Csp^2 atom pairs, and a peak located at 1350 cm^{-1} (D peak) due to a vibration with A_{1g} symmetry, not present in perfect graphite and existing only in disordered carbon structures. The selection of the vibration modes is broken due to a disorder and defects existing in the graphitic lattice (increase of the ratio edge planes/basal planes, decrease of the size of the crystallites, grain boundaries, amorphous carbon, doping). D mode is dispersive, as it varies with photon excitation energy, whereas the G peak is not dispersive [24]. The Raman spectra of the fibers show the two main D and G peaks and some minor features usually located around 1100–1200 cm^{-1} (Fig. 2). The peak located around 1100–1200 cm^{-1} correspond to modes that are roughly a combination of a stretching of a chain containing vinyl groups and C—H wagging modes, heteroatoms and sp^2 carbon atoms located in defects and in an amorphous phase. It cannot be assigned to any sp^3 bonded phase, as it is sometimes referred in the analysis of diamond-like structures [25,26], because this peak is dispersive with excitation energy [27]. Ferrari and Robertson [27,28] concluded that this type of fitting may not be the most appropriate assignment, even if it has been routinely used for the fitting of Raman spectra of carbon materials. They also suggested that the peak located at 1200 cm^{-1} could be included in the G peak if the latter was fitted with a Breit–Wigner–Fano line (asymmetric line shape) instead of a Gaussian. The location of the peaks was not fixed, so that the fitting could be as close as possible to the experimental spectra. The location of the peaks did not change significantly with oxidative surface treatment. A peak with very small intensity located at 2335 cm^{-1} was observed for all fibers. It is commonly named G* band and originates from a combination of the different phonon modes in graphene like structures [29]. Lastly, a wide peak centered around 2900 cm^{-1} was also present in each spectra and is the combination of two main component peaks. A first component peak is located at 2640 cm^{-1}, and is commonly named 2D band or G′ band. It comes from a double resonance Raman process and has a close correlation with the electronic band structures existing in graphite like materials [29], and it is also the overtone of the D band [30]. A second peak located at 2950 cm^{-1} corresponds to glassy carbon structures.

The fitting of the region of the spectra between 1000 cm^{-1} and 1800 cm^{-1} with three peaks components (peak D, peak G and the peak located at 1100–1200 cm^{-1}, named peak C–H in this study) is displayed in Fig. 2.

Oxidative post-treatments create some disorder whose nature is different from the one already existing in low ordered graphitic materials like high strength carbon fibers. That disorder can be quantified by the FWHM of the peaks and the ratio $I_D/(I_D+I_G)$ or I_D/I_G, I_D and I_G being respectively the intensities of the D and G peaks. Compared to X-ray diffraction, Raman spectroscopy is less sensitive to the interlayer distance between graphitic layers but is more sensitive to a change of the order existing in the graphitic structure [31].

Cuesta and al. [31] explained that an increase of the ratio $I_D/(I_D+I_G)$ without any enlargement of the FWHM of the peaks meant that edge planes were created. For each type of fiber, the surface treatment systematically led to an increase of the ratio $I_D/(I_D+I_G)$ without a significant change of the FWHM of the peaks. The thermochemical surface treatment created edge planes at the surface of every type of fiber. The value of the parameter L_a obtained

Table 4
Evolution of disorder in the surface graphitic structure and evolution of the size of the crystals after surface treatment.

	I_D/I_G	$I_D/(I_D+I_G)$	L_a (nm)
Hextow® IM 10	2.116 ± 0.017	0.679 ± 0.002	8.0
Hextow® IM 10 surface treated	2.217 ± 0.047	0.689 ± 0.005	7.6
Hextow® IM 7	2.195 ± 0.037	0.687 ± 0.004	7.7
Hextow® IM 7 surface treated	2.252 ± 0.038	0.692 ± 0.004	7.5
Hextow® AS4	2.138 ± 0.037	0.681 ± 0.004	7.9
Hextow® AS4 surface treated	2.225 ± 0.041	0.689 ± 0.003	7.6
Panex® 35	2.045 ± 0.046	0.678 ± 0.004	7.6
Panex® 35 surface treated	2.288 ± 0.025	0.696 ± 0.002	7.2
Textile grade	2.265 ± 0.020	0.694 ± 0.002	7.4
Textile grade surface treated	2.418 ± 0.049	0.707 ± 0.004	7.0

by X-ray diffraction being larger than 2 nm, the Tuinstra–Koenig equation could be used to calculate the value of L_a for each sample [28].

$$R(\lambda) = \frac{I_D}{I_G} = \frac{C(\lambda)}{L_a} \quad \text{with } C(\lambda) = 16.82\,\text{nm for } \lambda = 514.5\,\text{nm [26]}.$$

The value of L_a before and after surface treatment for each type of fiber is reported in Table 4. The thermochemical surface treatment decreased the size of the crystals in every case, along with an increase of the disorder in the graphitic structure. Moreover, the smaller the original crystal size, the more it generally decreased after surface treatment (Fig. 3). As seen in Fig. 3, textile and industrial based Panex® 35 carbon fibers are influenced more than aerospace grade carbon fibers. Despite the creation of those defects in the graphitic layers of the surface, a healing effect was observed when measuring the tensile strength of the fibers before and after surface treatment [11]. It appears that this increase of the tensile strength was due to the removal or smoothing of large voids that are more likely to initiate the failure of fibers [11]. When it comes to the evolution of the ratio I_D/I_G, a clear difference was observed between the types of PAN precursor. Indeed, the relative increase of the ratio I_D/I_G was higher for the fibers made with textile grade PAN precursor. The thermochemical surface treatment created more defects in the graphitic structures that were already the least organized. The original density of defects of the surface had a clear impact on the final state of the graphitic structure after surface treatment, which implies that the concentration of oxygen should be higher with the fiber made of textile grade PAN fiber. The evolution of the surface chemistry for all types of fibers was then studied by XPS.

Table 5
Elemental composition before and after surface treatment determined by XPS analysis.

	C (%)	O (%)	N (%)
Hextow® IM 10 surface treated	84	14	2
Hextow® IM 10 commercial surface treatment	90	7	3
Hextow® IM 7 surface treated	81	15	4
Hextow® IM 7 commercial surface treatment	87	7	6
Hextow® AS4 surface treated	81	16	3
Hextow® AS4 commercial surface treatment	89	8	3
Panex® 35 surface treated	77	20	3
Panex® 35 commercial surface treatment	88	7	5
Textile grade PAN surface treated	73	24	3

3.3. X-ray photoelectron spectroscopy

The typical spectra obtained with textile grade PAN carbon fibers before and after surface treatment are displayed in Fig. 4. The elemental compositions, before and after surface treatment and for all types of fibers, are presented in Table 5. All surfaces were constituted of carbon, oxygen and nitrogen only. It was clear that the final concentration of oxygen that was obtained with fibers made with textile grade PAN precursor were superior to the ones obtained with aerospace grade PAN fibers. The concentrations obtained with aerospace grade PAN fiber were similar and comprised between 14% and 16%. The concentration of oxygen obtained with the thermochemical surface treatment was systematically higher (around two times) than the one obtained with the commercial electrochemical surface treatment (fibers surface treated and not sized were provided by the manufacturers) (Table 5). The results demonstrated a clear relationship between the final content of oxygen and

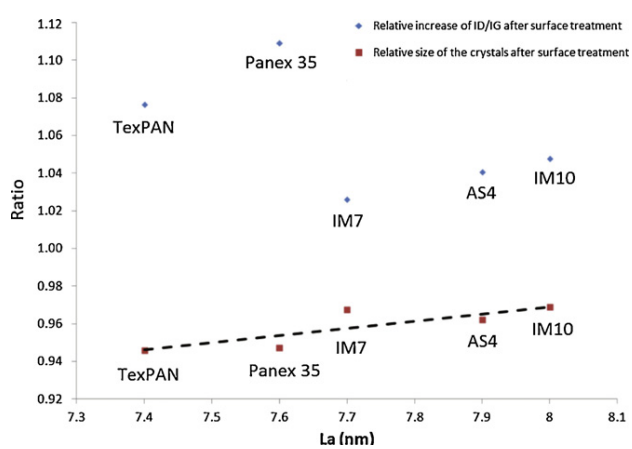

Fig. 3. Evolution of the relative size of L_a and evolution of I_D/I_G as a function of L_a after surface treatment.

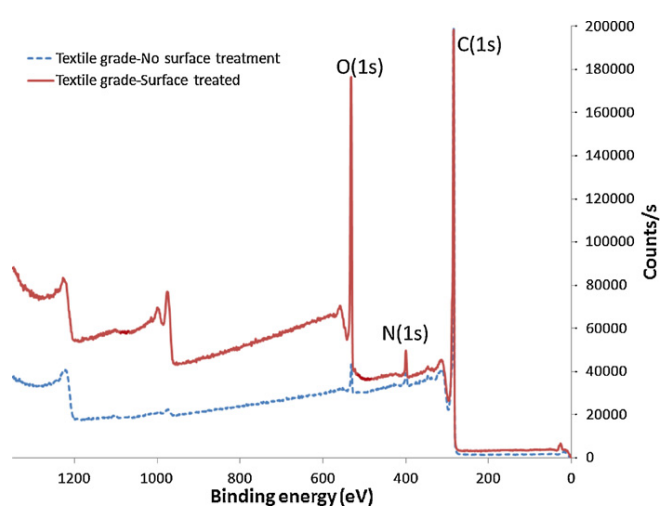

Fig. 4. XPS spectra of textile grade PAN fibers before and after the thermochemical surface treatment.

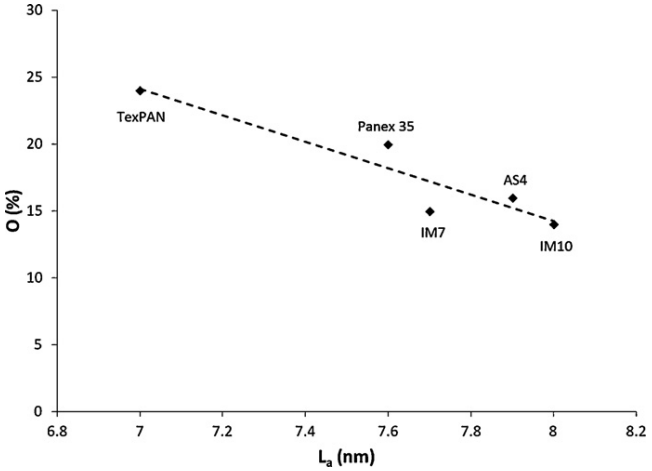

Fig. 5. Oxygen content at the surface of fibers after thermochemical surface treatment as a function of crystal length (L_a).

the size of the crystals before surface treatment, in the case of the thermochemical surface treatment. The smaller the crystal size, the higher the final content of oxygen at the surface of the fibers (Fig. 5). A smaller size for the crystals corresponds to a higher surface of the grain boundary layers between crystals, which represents a higher density of defects in the graphitic structure of the surface of the fiber. Moreover, the surface treatment further increased the density of defects at the surface. The content of oxygen was also associated with an increase of the ratio I_D/I_G determined by Raman spectroscopy (Fig. 6). The textile grade and industrial PAN based fibers showed higher content of oxygen after surface treatment but also a higher relative increase of disorder density in the graphite-like structure of the surface.

The fitting of the C(1s), O(1s) and N(1s) peaks allowed an analysis of the surface chemistry generated by the thermochemical surface treatment as a function of the type of fiber (Table 6). The fitting of Panex® 35 fibers surface treated by the thermochemical surface treatment is displayed in Fig. 7 as an example. Our group previously reported that the thermochemical surface treatment was preferentially generating hydroxyl groups and carboxylic acid functionalities and barely any carbonyl groups (Panex® 35 fibers) [11]. A better control of the surface chemistry was achieved when compared to the commercial electrochemical surface treatment. The same observation was made with the Hextow® fibers

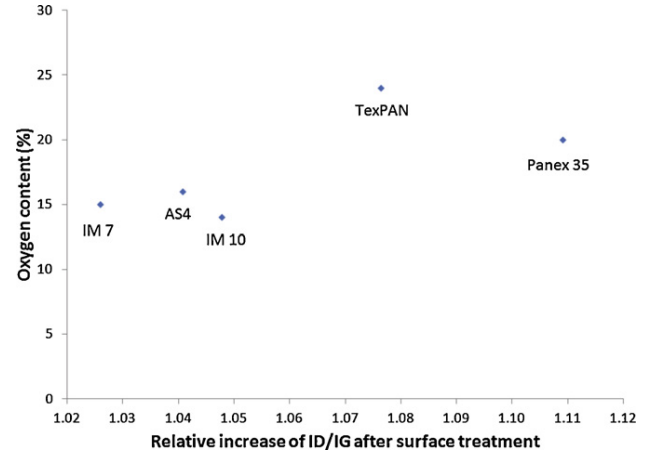

Fig. 6. Relationship between the creation of surface disorder in the graphitic structure and the final content of oxygen measured by XPS analysis.

Table 6
Relative area of each component peak in the fitting of C(1s), O(1s) and N1(S) peaks, in percentage of the total area of the peak.

Fibers	C(1s)									O(1s)						N(1s)			
	Csp^2	Csp^3	C—COOR	C—N	C—O—R	C=O	COOR	H_2O	Ph=O, Ph—C=O	C=O	R—OH, C—O—C	Ph—OH, C—O	H_2O phys	H_2O chem	Pyridine	Amides, amines, C—N	Pyridone	Pyridinium, N^+
Hextow® IM 10 surface treated	77	5	4	1	5	2	4	2	16	16	35	23	5	5	24	14	22	40
Hextow® IM 10 commercial surface treatment	83	7	2	2	1	2	2	1	25	39	5	27	2	2	22	32	22	24
Hextow® IM7 surface treated	74	5	5	2	7	1	5	1	25	37	16	18	3	1	29	14	29	28
Hextow® IM7 commercial surface treatment	80	5	2	4	3	2	2	2	45	8	27	11	4	5	17	33	28	22
Hextow® AS4 surface treated	76	4	4	3	5	2	4	2	20	34	20	20	4	2	20	16	35	29
Hextow® AS4 commercial surface treatment	84	2	3	2	4	1	3	1	38	13	28	14	4	3	15	21	33	31
Panex 35® surface treated	75	2	6	2	5	3	6	1	20	24	14	34	4	4	25	8	30	37
Panex 35® commercial surface treatment	81	2	2	6	3	3	2	1	27	12	19	32	5	5	14	32	28	26
Textile grade	48	11	13	1	12	0	13	2	17	40	0	35	3	5	13	28	34	25

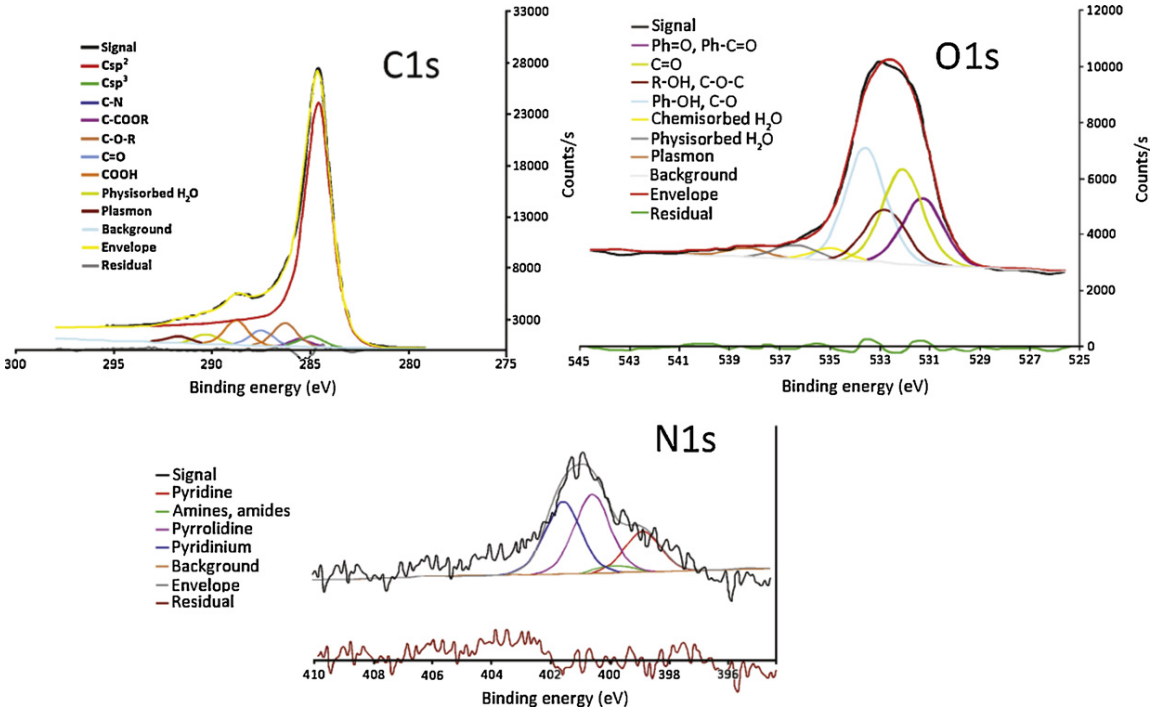

Fig. 7. Fitting of the C(1s), O(1s) and N(1s) peaks. Panex® 35 fibers surface treated with the thermochemical surface treatment [11].

and with the TexPAN fibers, which means that it did not depend on the grade of the PAN precursor. The continuous surface treatment technology presented here is then very attractive for epoxy composite applications, as hydroxyl groups and carboxylic acid functionalities have the potential to create covalent bonding with epoxy matrices. It can also be an optimized surface treatment for the grafting of coupling agents meant to create covalent bonding with other types of matrices (vinyl esters, polyesters, acrylate, . . .). The fitting of the O(1s) peak confirmed the generation of carboxylic acid functionalities and also showed that the nature of the hydroxyl groups generated at the surface of textile grade PAN fibers corresponded to phenol functionalities in majority, whereas the relative area of the component related to alcohol functionalities was higher with aerospace grade PAN fibers (but it is necessary to take into consideration that it could be ether-like functionalities as well). The surface chemistry generated by the different electrochemical surface treatments could be quite different when it comes to the nature of the oxygen-containing functionalities. Each carbon fiber manufacturer has developed its own technology regarding electrochemical surface treatment. When it comes to nitrogen-containing functionalities, the fitting of the N(1s) peak confirmed the fact that the thermochemical surface treatment did not generate much dangling functionalities like amines and amides in comparison to electrochemical surface treatments. Indeed, the grafting of amine functionalities is purposely targeted by the carbon fiber manufacturers for epoxy applications [32]. But the thermochemical surface treatment in this study is aimed at generating oxygen-containing functionalities only. All in all, the continuous thermochemical surface treatment characterized in this study was found to be more efficient as compared to conventional electrochemical surface treatment for the functionalization of different carbon fibers microstructures and particularly suitable for textile grade PAN fibers, which are destined to be used in very high production volumes of carbon fiber reinforced composite parts, like in the automotive industry.

4. Conclusions

A continuous thermochemical surface treatment was applied to carbon fibers made with different grades of PAN precursor. The final surface concentration of oxygen was directly related to the grade of the PAN precursor and to the size of the crystals (more precisely to the average microstructural parameters of the graphitic structure L_a), which was itself a function of the grade of the PAN precursor. The higher concentration of oxygen-containing functionalities were obtained with textile grade PAN fibers. The preferential creation of hydroxyl groups and carboxylic acids was confirmed regardless of the type of carbon fiber, which provides a higher level of desirable functionalities in comparison to the commercial electrochemical surface treatments. The thermochemical surface treatment is more appropriate when those functionalities have a strategic role in the establishment of effective interfacial adhesion, for epoxy based applications for instance. The thermochemical surface treatment has proved to be a very effective dry alternative to the conventional wet electrochemical surface treatment for the production of all types of studied carbon fibers.

Acknowledgements

This research was sponsored by the U.S. Department of Energy, Assistant Secretary for Energy Efficiency and Renewable Energy, Office of Vehicle Technologies, as part of the Lightweighting Materials Program. A part of this research was done through the Oak Ridge National Laboratory's High Temperature Materials Laboratory User Program, sponsored by the U.S. Department of Energy, Office of Energy Efficiency and Renewable Energy, Vehicle Technologies Program and through the Shared Research Equipment (SHaRE) User Facility operated for the U.S. Department of Energy Office of Science by the Oak Ridge National Laboratory. Authors would like to thank Dr. Tomonori Saito for his valuable discussions and comments. Authors would like to thank Mr. Truman Bond and ReMaxCo

Technologies LLC for their indispensible contribution to the development of the surface treatment technology. Zoltek and Hexcel are sincerely thanked for providing carbon fibers.

References

[1] F. Vautard, P. Fioux, L. Vidal, J. Schultz, M. Nardin, B. Defoort, Influence of the carbon fiber surface properties on interfacial adhesion in carbon fiber–acrylate composites cured by electron beam, Composites Part A: Applied Science and Manufacturing 42 (2001) 859–867.
[2] C.W. Jennings, Surface roughness and bond strength of adhesives, Journal of Adhesion 4 (1972) 25–38.
[3] V.K. Raghavendran, L.T. Drzal, P. Askeland, Effect of surface oxygen content and roughness on interfacial adhesion in carbon fiber-polycarbonate composites, Journal of Adhesion 16 (2002) 1283–1306.
[4] D.K. Owens, R.C. Went, Estimation of the surface free energy of polymers, Journal of Applied Polymer Science 13 (1969) 1741–1747.
[5] F.M. Fowkes, Role of acid–base interfacial bonding in adhesion, Journal of Adhesion Science and Technology 1 (1987) 7–27.
[6] K.J. Hook, R.K. Agrawal, L.T. Drzal, Effects of microwave processing on fiber-matrix adhesion. 2. Enhanced chemical bonding epoxy to carbon-fibers, Journal of Adhesion 32 (1990) 157–170.
[7] M.M. Pastor-Blas, M.S. Sanchez-Adsuar, J.M. Martin-Martinez, Weak boundary layers in styrene-butadiene rubber, Journal of Adhesion 50 (1995) 191–210.
[8] M.C. Paiva, M. Nardin, C.A. Bernardo, J. Schultz, Influence of thermal history on the results of fragmentation tests on high-modulus carbon-fiber/polycarbonate model composites, Composites Science and Technology 57 (1997) 839–843.
[9] F. Vautard, L. Xu, L.T. Drzal, Influence of cure volume shrinkage on interfacial adhesion in carbon fiber-vinyl ester composites, in: Extended abstracts, International SAMPE'09 Conference and Exhibition, Baltimore (Maryland, USA), Society for the Advancement of Material and Process Engineering, 2009, pp. 1–13.
[10] L.T. Drzal, M.J. Rich, P.F. Lloyd, Adhesion of graphite fibers to epoxy matrices: I. The role of fiber surface treatment, Journal of Adhesion 16 (1982) 1–30.
[11] F. Vautard, S. Ozcan, H. Meyer, Properties of thermo-chemically surface treated carbon fibers and of their epoxy and vinyl ester composites, Composites Part A: Applied Science and Manufacturing 43 (2012) 1120–1133.
[12] H.P. Klug, L.E. Alexander, X-ray Diffraction Procedures, John Wiley, New York, 1954, p. 491.
[13] B.E. Warren, X-ray Diffraction, Addison-Wesley, Reading, Massachusetts, 1969, p. 258.
[14] B.E. Warren, P. Bodenstein, The shape of two-dimensional carbon black reflections, Acta Crystallographica 20 (1966) 602–605.
[15] J.I.B. Wilson, J.S. Walton, G. Beamson, Analysis of chemical vapour deposited diamond films by X-ray photoelectron spectroscopy, Journal of Electron Spectroscopy 121 (2001) 183–201.
[16] S.T. Jackson, R.G. Nuzzo, Determining hybridation differences for amorphous carbon from the XPS C1s envelope, Applied Surface Science 90 (1990) 195–203.
[17] U. Zielke, K.J. Hüttinger, W.P. Hoffman, Surface oxidized carbon fibers: II. Chemical modification, Carbon 34 (1996) 999–1005.
[18] S. Biniak, G. Szymański, J. Siedlewski, A. Światkowski, The characterization of activated carbons with oxygen and nitrogen surface groups, Carbon 35 (1997) 1799–1810.
[19] M.R. Alexander, F.R. Jones, Effect of electrolytic oxidation upon the surface chemistry of type a carbon fibers. 3. Chemical state, source and location of surface nitrogen, Carbon 34 (1996) 1093–1102.
[20] P. Morgan, Carbon Fibers and Their Composites, CRC Press, 2005.
[21] P. Lespade, A. Marchand, Caractérisation de matériaux carbonés par microspectroscopie Raman, Carbon 22 (1984) 375–385.
[22] O. Bessac, B. Goffé, J.P. Petitet, E. Froigneux, M. Moreau, J.N. Rouzaud, On the characterization of disordered and heterogeneous carbonaceous materials by Raman spectroscopy, Spectrochimica Acta Part A 59 (2003) 2267–2276.
[23] T.P. Mernagh, R.P. Cooney, R.A. Johnson, Raman spectra of graphon carbon black, Carbon 22 (1984) 39–42.
[24] I. Pócsik, M. Hundhausen, M. Koós, L. Ley, Origin of the D peak in the Raman spectrum of microcrystalline graphite, Journal of Non-Crystalline Solids 227–230 (1998) 1083–1086.
[25] W.A. Yarbrough, R. Messier, Current issues and problems in the chemical vapor deposition of diamond, Science 247 (1990) 688–696.
[26] D.S. Knight, W.B. White, Characterization of diamond films by Raman spectroscopy, Journal of Materials Research 4 (1989) 385–393.
[27] A.C. Ferrari, J. Robertson, Origin of the 1150 cm^{-1} Raman in nanocrystalline diamond, Physical Review B 63 (2001), 121405(R).
[28] A.C. Ferrari, J. Robertson, Interpretation of Raman spectra of disordered and amorphous carbon, Physical Review B 6 (2000) 14095–14106.
[29] D. Yoon, H. Moon, H. Cheong, J.S. Choi, J.A. Choi, B.H. Park, Variations in the Raman spectrum as a function of the number of graphene layers, Journal of Korean Physical Society 55 (2000) 1299–1303.
[30] M.A. Pimenta, G. Dresselhaus, M.S. Dresselhaus, L.G. Cançado, A. Jorio, R. Saito, Studying disorder in graphite-based systems by Raman spectroscopy, Physical Chemistry Chemical Physics 9 (2007) 1276–1291.
[31] A. Cuesta, P. Dhamelincourt, J. Laureyns, A. Martínez-Alonso, J.M.D. Tascón, Raman microprobe studies on carbon materials, Carbon 32 (1994) 1523–1532.
[32] K. Mason, Advances in sizings and surface treatment for carbon fibers, High Performance Composites (2004).

All in-text references underlined in blue are linked to publications on ResearchGate, letting you access and read them immediately.